Investigating the Scale Adaptivity of a Size-Filtered Mass Flux Parameterization in the Gray Zone of Shallow Cumulus Convection

MAREN BRAST, VERA SCHEMANN, AND ROEL A. J. NEGGERS

Institute for Geophysics and Meteorology, University of Cologne, Cologne, Germany

(Manuscript received 8 August 2017, in final form 19 December 2017)

ABSTRACT

In this study, the scale adaptivity of a new parameterization scheme for shallow cumulus clouds in the gray zone is investigated. The eddy diffusivity/multiple mass flux [ED(MF)^n] scheme is a bin-macrophysics scheme in which subgrid transport is formulated in terms of discretized size densities. While scale adaptivity in the ED component is achieved using a pragmatic blending approach, the MF component is filtered such that only the transport by plumes smaller than the grid size is maintained. For testing, ED(MF)^n is implemented into a large-eddy simulation (LES) model, replacing the original subgrid scheme for turbulent transport. LES thus plays the role of a nonhydrostatic testing ground, which can be run at different resolutions to study the behavior of the parameterization scheme in the boundary layer gray zone. In this range, convective cumulus clouds are partially resolved. The authors find that for quasi-equilibrium marine subtropical conditions at high resolutions, the clouds and the turbulent transport are predominantly resolved by the LES. This partitioning changes toward coarser resolutions, with the representation of shallow cumulus clouds gradually becoming completely carried by the ED(MF)^n. The way the partitioning changes with grid spacing matches the behavior diagnosed in coarse-grained LES fields, suggesting that some scale adaptivity is captured. Sensitivity studies show that the scale adaptivity of the ED closure is important and that the location of the gray zone is found to be moderately sensitive to some model constants.

1. Introduction

Clouds play an important role in Earth's climate system. While global weather prediction models resolve large-scale clouds, smaller-scale clouds require parameterization. This includes shallow cumulus clouds that cover large areas over the oceans in the subtropical trade wind regions. The vertical transport of heat and water vapor associated with shallow cumulus clouds is a key part of the Hadley circulation and thus significantly affects large-scale circulation (e.g., Tiedtke 1989; Neggers et al. 2007). The importance of correctly representing this type of cloud in large-scale models has long been recognized (Tiedtke 1989; Vial et al. 2013), and a variety of parameterizations have been developed [an overview of cumulus parameterizations is given in Arakawa (2004)]. Limits in computational power still constrain the complexity of such parameterizations, so in practice, a compromise must be found between a realistic cloud representation and computational costs.

First-generation cumulus schemes are often based on the bulk mass flux approach (e.g., Ooyama 1971; Betts 1973; Yanai et al. 1973; Arakawa and Schubert 1974; Fritsch and Chappell 1980; Tiedtke 1989). In this approach, the vertical transport of heat and moisture by an ensemble of rising plumes is parameterized through one single plume representing the whole ensemble (Simpson and Wiggert 1969). Mass flux schemes are popular because they are not only relatively simple and computationally cheap but they also capture key aspects of cumulus convection such as the advective nature of related transport. A mass flux parameterization can represent most of the turbulent convective transport in the cloud layer (Siebesma and Cuijpers 1995; Siebesma et al. 2003) as well as the coupling with the subcloud layer (Grant 2001). The development and further improvement of mass flux schemes is ongoing, with the rising plume model (Simpson and Wiggert 1969) still at the foundation of most of these frameworks.

When the grid resolution of atmospheric models increases, boundary layer processes become partially resolved [a situation referred to as the ''terra incognita'' or ''gray zone'' of convection (Wyngaard 2004)]. How

Corresponding author: Roel A. J. Neggers, neggers@meteo.uni-koeln.de

DOI: 10.1175/JAS-D-17-0231.1

to represent such circulations with parameterization schemes is an open question (Zhou et al. 2014). Previous studies have shown that for model resolutions within the gray zone, unrealistic flow characteristics develop (e.g., Zhou et al. 2014; Ching et al. 2014). An ideal parameterization scheme should be able to introduce realistic interactions between unresolved and resolved circulations. Such a parameterization should be scale aware and scale adaptive. This means that the scheme should be aware which processes should be parameterized and which can be expected to be resolved by the host model, which is called ''scale awareness.'' When a scheme is not only aware of the scale of resolved processes but is also able to adapt and only represent those processes that are not resolved, then this scheme is called ''scale adaptive.'' Scale awareness and adaptivity can be introduced by using not a single but multiple plumes, each representing the characteristics of plumes of a certain size, and then filtering them depending on the grid size. This use of multiple plumes leads to more degrees of freedom and the possibility of interaction between the plumes, a simple form of population dynamics (Neggers 2015). The idea of parameterizing shallow cumulus convection by taking into account clouds of different sizes is not new. One of the first to use this idea are Arakawa and Schubert (1974), who divide an ensemble of shallow cumulus clouds into subensembles and thereby account for the different cloud sizes. This scheme is the basis for the multiparcel scheme by Wagner and Graf (2010), who use a different closure formulation than Arakawa and Schubert (1974). Neggers et al. (2002) describe a multiparcel model with the focus on the lateral entrainment rate, which depends on the vertical velocity of the rising parcels. Park (2014) uses multiple updrafts and downdrafts to unify deep and shallow convection. Other schemes use ensembles of clouds within a stochastic approach (e.g., Ooyama 1971; Plant and Craig 2008; Sakradzija et al. 2015). Some recent studies are specifically designed to introduce the ability to adapt to different resolutions (Teixeira et al. 2008; Bogenschutz and Krueger 2013; Boutle et al. 2014). While encouraging progress is reported by these studies, to make further progress, more insight is still needed into the exact nature of the size dependence of turbulence within the gray zone and how this dependence can best be parameterized.

The use of probability density functions as a function of eddy size in shallow cumulus parameterization has recently received renewed attention, as it brings several potential advantages for parameterization in the gray zone. Bulk mass flux approaches describe the characteristics of one single cloud that represents the whole ensemble of cumulus clouds. However, shallow cumulus clouds vary greatly in size and therefore have different characteristics (e.g., Dawe and Austin 2012; Böing et al. 2012), so combining the characteristics of all individual clouds into one bulk scheme fails to realistically describe the variation among the clouds. A scheme using size densities can take the characteristics of different cloud sizes into account, as well as representing the distribution of cloud sizes, which is important because in a shallow cumulus field, many small clouds and few large clouds exist (e.g., Plank 1969). Another advantage of using size densities is that, in principle, the different cloud sizes can interact with each other indirectly through the environment in which they rise (i.e., through the mean state of the columns in the large-scale model). Brast et al. (2016) show that the fate of rising plumes in a heterogeneous environment is predominantly determined by local mixing, so hostile (friendly) environments can effectively terminate (accelerate) their ascent. Thus, when such a subgrid parameterization based on rising plumes is capable of locally changing its environment, it can create heterogeneity and affect other plumes in its vicinity. Finally, with size densities, it is easy to introduce scale awareness into the parameterization by only taking the desired cloud sizes into account.

This study focuses on the opportunity to introduce scale adaptivity provided by boundary layer schemes that are formulated in terms of discretized size densities. More specifically, we make use of the eddy diffusivity/multiple mass flux [ED(MF)^n] scheme as proposed and described by Neggers (2015). In Neggers (2015), ED(MF)^n was implemented into a single-column model and compared to a large-eddy simulation (LES), which is a common method to develop and test parameterization schemes, building on the fact that LES has proven to be successful at simulating moist convective boundary layers and clouds (Siebesma et al. 2003; Heus et al. 2010; vanZanten et al. 2011). In this study, the scale adaptivity of ED(MF)^n is tested in an altogether different way. Instead of using offline diagnostics to evaluate parameterizations, the scheme is implemented into an LES as a subgrid scheme. The key advantages of this method are that (i) the scheme is tested interactively with the resolved flow and that (ii) the discretized LES equations are used as a simple nonhydrostatic testing ground for investigating scale adaptivity. Most previous studies using the LES interactively have focused on the dry convective boundary layer (e.g., Beare 2014; Efstathiou and Beare 2015), while we are focusing on a shallow cumulus scheme. In addition, while most previous studies have focused on scale adaptivity in the diffusive transport models (e.g., Boutle et al. 2014; Efstathiou and Beare 2015; Bhattacharya and Stevens 2016), this study

is concerned with scale adaptivity in advective mass flux models. This topic has received considerably less attention, with a few recent exceptions (e.g., Arakawa et al. 2011; Sakradzija et al. 2016). In this study, the original subgrid scheme (SGS) for subgrid-scale transport of the conserved thermodynamic state variables of the University of California, Los Angeles (UCLA), LES model (Stevens et al. 2005) is replaced with the parameterization scheme ED(MF)^n. This means that the boundary layer scheme is active within each column of the LES grid. The LES is then run with resolutions varying from 100 to 1000 m, covering the boundary layer gray zone. Note that, at such large grid spacings, the largest boundary layer eddies remain unresolved, so the simulation can no longer be named an LES. However, in that range, it can be interpreted as an idealized nonhydrostatic large-scale model, in which the turbulent transport is done by ED(MF)^n. Thus, LES is used as an interactive testing ground for scale-aware and scale-adaptive modeling. By launching multiple plumes in each column, the LES acts as a simplified larger-scale model with varying resolutions, profiting from its nonhydrostatic formulation and high model transparency. The main goal of this study is to investigate if and how the partitioning of the transport between resolved and parameterized scales takes place when size filtering is introduced into ED(MF)^n and how the plume model responds to resolved clouds present in an LES domain at different resolutions of the LES.

In section 2, the ED(MF)^n scheme and the method of testing its scale adaptivity are described in detail. In section 3, the problems connected to simulating in the gray zone are described. The behavior of ED(MF)^n as a scale-adaptive subgrid scheme in LES is explored in section 4, and a discussion and summary of the findings are given in section 5.

2. Method

a. Formulation of ED(MF)^n

The ED(MF)^n framework used in this study is based on the eddy diffusivity/mass flux (EDMF) framework (Siebesma and Teixeira 2000; Soares et al. 2004; Siebesma et al. 2007). EDMF parameterizes the transport in the boundary layer by combining two previously used approaches. The ED part represents the local, downgradient vertical transport by turbulence at smaller scales, which is parameterized by multiplying the local gradient of Φ with a coefficient K, where Φ is a conserved thermodynamic variable (liquid water potential temperature Θ_l or total water mixing ratio q_t). The MF part describes the nonlocal advective vertical transport by turbulence at the larger scales within the boundary layer. MF is parameterized by the difference between the Φ of the updraft and the horizontal mean multiplied by a mass flux M. The mass flux approach is capable of representing convective clouds, so the combination of both parts can in principle be used to describe both clear and cloudy convective boundary layers, as well as transitions between the two. The original framework of EDMF applies one bulk updraft to describe the total vertical flux by all thermals in the gridbox. Many different parameterization schemes have been developed based on the original EDMF framework (e.g., Neggers et al. 2009; Angevine et al. 2010; Sušelj et al. 2012, 2013; Sakradzija et al. 2016). To make EDMF applicable in the gray zone of boundary layer convection, Neggers (2015) recently formulated a size-dependent multiplume version of EDMF. Each plume represents the net properties of a single bin from a discretized size distribution of convective thermals. In effect, this constitutes a ''bin macrophysics'' framework, which in principle allows the size filtering of the underlying size density of advective thermals. In this framework, ED(MF)^n, the vertical transport Φ is parameterized by

$$\overline{w'\Phi'}(z) = -K_h(z)\frac{\partial\overline{\Phi}(z)}{\partial z} + \sum_{l=0}^{F}\mathscr{M}(l,z)[\Phi_u(l,z) - \Phi_e(z)]\Delta l, \tag{1}$$

with filter size F, size bins l, the characteristics of the environment and the updrafts as subscripts e and u, respectively, and heat as subscript h because we only apply ED(MF)^n for thermodynamic variables. The horizontal dependency (x, y) has been left out here to simplify the notation. The first term on the right-hand side represents the local downgradient transport by diffusive processes to the smallest scales; the second term represents the nonlocal advective mass flux by the largest thermals. This formulation allows ED(MF)^n to be applied at different resolutions by only integrating over those plumes that are too small to be resolved. In Eq. (1), $\mathscr{M}$ is the volumetric mass flux:

$$\mathscr{M}(l,z) = \mathscr{A}(l,z)[w(l,z) - w_e(z)], \tag{2}$$

with w_e the vertical velocity of the environment. In large-scale models, the horizontal mean of w is considered, which is negligible (e.g., Siebesma et al. 2007). However, a key difference from the bulk EDMF approach is that w_e is considered instead of the horizontal mean $\overline{w}$; the same applies to the thermodynamic state ϕ_e. The motivation for this step is that in the gray zone, some of the bigger thermals become resolved, so the vertical velocity of the environment in which a plume

rises can become significant (Honnert et al. 2016). Since the vertical velocity of the environment in our case is the resolved vertical velocity of the LES, w_e becomes w_{LES}. Correspondingly, Φ_e becomes Φ_{LES}. The calligraphic symbols represent variables that are size dependent, thus representing probability density functions as a function of size. The area density $\mathscr{A}$ is the area covered by all the plumes in one bin:

$$\mathscr{A}(l,z) = \frac{\mathscr{N}(l,z)\Lambda_a(l,z)l^2}{A}, \tag{3}$$

with $\mathscr{N}$ representing the number of plumes for each size, A the horizontal area of the gridbox, and Λ_a describing the vertical structure of $\mathscr{A}$. The total area covered by advective, surface-driven plumes is given by

$$a(z) = \sum_{l=0}^{F} \mathscr{A}(l,z)\Delta l. \tag{4}$$

To close the set of Eqs. (1)–(4), the eddy diffusivity coefficient K_h and the behavior of the updrafts must be described. For the thermals, a plume model is used, based on Simpson and Wiggert (1969), which was also used in the original EDMF by Siebesma et al. (2007). This plume model includes the following size dependencies:

$$\frac{\partial \Phi(l,z)}{\partial z} = -\varepsilon(l)[\Phi(l,z) - \Phi_e(z)], \tag{5}$$

$$\frac{1}{2}(1-2\mu)\frac{\partial w^2(l,z)}{\partial z} = -b\varepsilon(l)\,[w^2(l,z) - w_e^2(z)] + B(l,z), \tag{6}$$

with $\mu = 0.15$ and $b = 0.5$ proportionality constants for drag (e.g., Romps and Charn 2015) and mixing, B the buoyancy, and ε the effective mixing rate; K_h is described in section 2c. Assumptions for the cloud size density $\mathscr{N}$, the area size a, and the entrainment of the plumes needed for the plume model are given in section 2b. For more details on the formulation of ED(MF)^n, see Neggers (2015). The formulation of ED(MF)^n differs from other schemes based on EDMF (e.g., Sušelj et al. 2012) in that (i) it is formulated in terms of discretized size densities, (ii) it has multiple plumes that are initialized individually at the surface, and (iii) the entrainment closure is size dependent (see section 2b). In particular, the size dependence at the foundation of the framework introduces new opportunities for scale-adaptive modeling of shallow cumulus clouds in the gray zone.

Figure 1 illustrates the concept of size filtering a discretized size density of advective plumes. The top panel shows a number of plumes of the parameterization scheme, each representing all updrafts of a certain size. Within one grid column, all these net plumes can in principle be active. Plumes can reach saturation and carry condensed water, thus representing cumulus clouds. In the bottom panel, the number of updrafts N present in each net plume is shown. A strong decrease in the plume number with size is shown, corresponding to the observed size distribution of shallow cumulus cloud fields (e.g., Plank 1969). The top panel also shows the lifting condensation level (LCL) of the plumes. Only the larger plumes condensate, while the termination height of the smaller plumes can be lower than the LCL. Also shown is the filter size. When implemented into a large-scale model, the model is run with a certain resolution, which determines the size of plumes that can be resolved. The filter size of ED(MF)^n can now be chosen to include only those plumes that are not resolved by the large-scale model, thus making the scheme scale aware.

b. A simplified scale-adaptive application of (MF)^n

Since the multiplume scheme is applied to a discretized size density featuring a limited number of plumes, a summation is used instead of an integral in Eq. (1). To use the scheme presented in section 2a, some assumptions must be made. One assumption concerns the entrainment rate ε of the plumes. In the literature, many dependencies have been suggested (e.g., Simpson and Wiggert 1969; Neggers et al. 2002; Kain and Fritsch 1990; Romps and Kuang 2010) depending on the definition of the entity that is entraining. A size dependence is established by many studies, both in laboratory (Turner 1962) and LES studies (e.g., Böing et al. 2012). The ED(MF)^n formulation uses a net effective entrainment to describe the net properties of a subpopulation of clouds of equal size regardless of life cycle stage. Neggers (2015) showed that in fair weather cumulus cloud fields, a clear size dependence exists in the net entrainment associated with this definition. Although observational evidence is currently missing and research is ongoing, for now, we assume that the size dependence is the dominant relation. This is sufficient for a first exploration of ED(MF)^n in the gray zone. Whether other dependencies are needed is a topic for future research. The size dependence used here is formulated as

$$\varepsilon(l) = \frac{c}{l}, \tag{7}$$

with c a proportionality constant, which we set to 1 for simplicity.

Our wish for model transparency also motivates the use of a simple, prescribed number density $\mathscr{N}(l, z)$. In

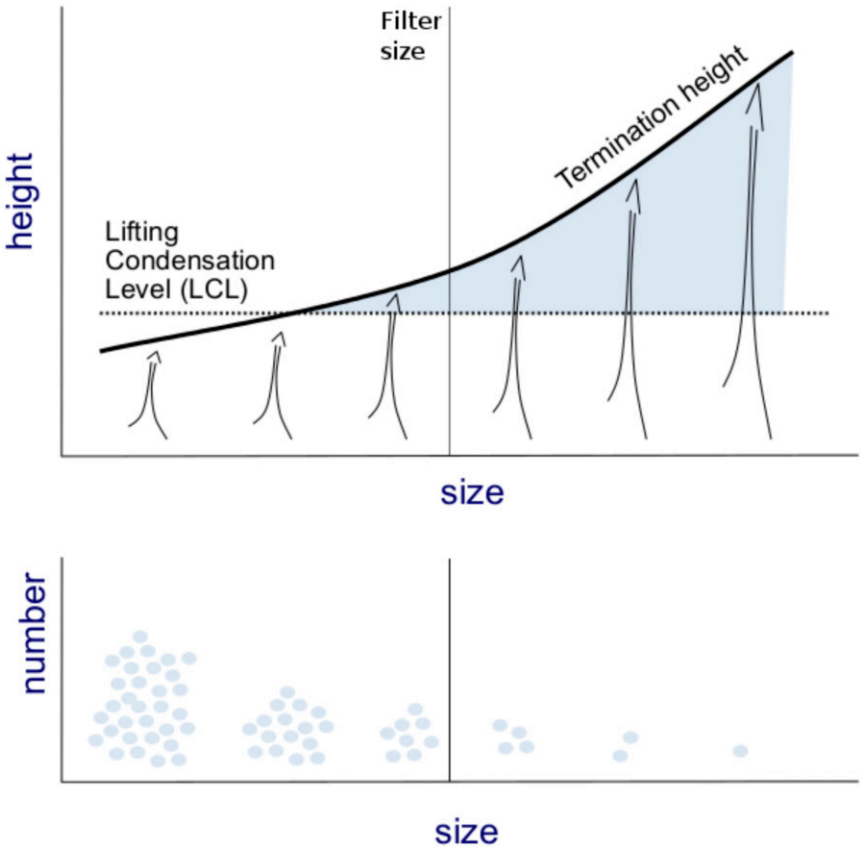

FIG. 1. Illustration of the concept of ED(MF)^n. (top) An ensemble of plumes with the LCL, termination height, and in blue the area where the plumes condense. (bottom) The number of updrafts represented by each plume in the top. Figure adapted from Neggers (2015).

reality, the number density changes significantly with time. This time evolution can express physical processes in the population average, such as cloud growth and organization, but also subsampling effects in the gray zone due to a too-small domain size. As our single purpose is to investigate the impact of size filtering, the use of a prescribed number density as a first step is appropriate.

In this paper, the size dependence in $\mathcal{N}(l, z)$ follows a power law without a scale break:

$$\mathcal{N}(l, z) = al^b, \tag{8}$$

with $b = -1.98$ the power-law exponent and a the constant of proportionality. The parameter a is obtained by assuming that the total area fraction covered by all plumes is always 10%. The full implications of this simplification are not yet fully understood, but it is sufficient as a first step. The sensitivity of a is studied in section 4c.

Finally, the vertical structure of each size bin is assumed to be constant with height while the plume is rising,

$$\Lambda_a(l, z) = \begin{cases} 1 & \text{for} \quad z \le z_t \\ 0 & \text{for} \quad z > z_t. \end{cases} \tag{9}$$

In effect, this means that within each size bin, the cloud number is assumed not to change with height. Above termination height, the net plume does not contribute to transport.

For each run, only those updrafts are taken into account that are smaller than the filter size F in Eq. (1). Up to now, F was assumed to be infinitely large so that transport at all sizes in the spectrum was included. The novelty of this study is that F can be smaller than infinity so that transport at sizes larger than F is excluded. We assume F is equal to the grid size. Although more than one grid box is needed to fully resolve a convective process (Skamarock 2004), this simplification represents a first step toward scale adaptivity, as it introduces true size filtering. Further research is needed to investigate how the structures at scales between the cutoff length and the effective resolution are affected. Further simplifications include that the updrafts can only rise vertically and horizontal displacement due to,

for example, the mean wind are not taken into account. Horizontal subgrid fluxes are also omitted and should be considered in future studies. Also, when the updrafts are calculated, they are given the instantaneous profiles of the LES columns in which the updrafts rise without taking the cloud life cycles into account. Note that life cycle information could be adopted into this formulation by introducing a time-varying N.

c. Application of ED

The main goal of this study is to investigate the scale adaptivity achieved by introducing scale awareness into the mass flux component. Nevertheless, some scale awareness also needs to be introduced into ED to avoid overaggressive diffusive mixing. This can, for example, occur near strong vertical gradients in the resolved state that are associated with the emergence of resolved (proto) cloud structures when entering the gray zone from the low-resolution side. This scale awareness is introduced by adjusting the coefficient K_h in Eq. (1).

The K parameterization is adjusted so that K_h consists of two components. One component consists of the K_h from the Smagorinsky–Lilly type scheme from the LES approach ($K_{h,\mathrm{LES}}$), which is best applicable at small grid spacings. The other component is formulated with K theory as applicable at large grid spacings ($K_{h,\mathrm{GCM}}$). The index GCM indicates that this formulation originates from global circulation models. The scale dependence of ED is introduced by pragmatic blending of the two components. In the subcloud layer, the blended K profile is always used, while in the cloud layer, the smaller one of the two components is applied.

The pragmatic blending approach by Boutle et al. (2014) adjusts the standard K profile by a weighting function. Thereby, at small resolutions, K_h resembles the $K_{h,\mathrm{LES}}$ calculated by the Smagorinsky-type scheme of the LES, while at coarse resolutions, K_h resembles the $K_{h,\mathrm{GCM}}$ calculated for a general circulation model:

$$K_h = WK_{h,\mathrm{GCM}} + (1 - W)K_{h,\mathrm{LES}}. \tag{10}$$

The $K_{h,\mathrm{LES}}$ originates from the LES model and is calculated as

$$K_{h,\mathrm{LES}} = \frac{K_m}{\mathrm{Pr}}, \tag{11}$$

with Pr the Prandtl number and K_m the coefficient for momentum:

$$K_m = (c_s l)^2 S\sqrt{1 - \frac{\mathrm{Ri}}{\mathrm{Pr}}}, \tag{12}$$

with c_s a constant, l a length scale, S the magnitude of deformation, and Ri the local Richardson number. For more information about the Smagorinsky–Lilly turbulence scheme, see, for example, Stevens et al. (1999).

The $K_{h,\mathrm{GCM}}$ is taken from the original ED(MF)^n, where the default K_h of the European Centre for Medium-Range Weather Forecasts (IFS documentation, cy40r1, part IV: Physical processes; www.ecmwf.int) is used. In the mixed layer,

$$K_{h,\mathrm{GCM}} = \frac{\kappa u_*}{\phi_{h0}}\left(1 - \frac{z}{z_i}\right)^2, \tag{13}$$

with κ the von Kármán constant, u_* the friction velocity, z the height, z_i the boundary layer height, and ϕ_{h0} a stability function.

The W is the weighting function based on turbulent kinetic energy partitioning by Honnert et al. (2011) and simplified by Boutle et al. (2014):

$$W = 1 - \tanh\left(\frac{\beta z_i}{\Delta x}\right)\max\left(0, 1 - \frac{\Delta x}{4z_i}\right), \tag{14}$$

with $\beta = 0.15$ a parameter controlling the speed of the transition, z_i the boundary layer height, and Δx the horizontal grid size.

Using Eq. (10), K_h resembles $K_{h,\mathrm{LES}}$ for the simulation with a horizontal resolution of 100 m, while K_h resembles $K_{h,\mathrm{GCM}}$ for a resolution of 1000 m. By using this blending approach and therefore including the grid size Δx, both parts of ED(MF)^n are now scale aware. The effect of this added change to ED(MF)^n is presented in section 4c.

d. Setup

The parameterization scheme ED(MF)^n as described above is implemented into an LES. The LES used in this study is the UCLA LES, described in Stevens et al. (2005). The UCLA LES parameterizes the subgrid fluxes with the Smagorinsky–Lilly closure. At the surface, the sea surface temperature and gradients are prescribed. The standard microphysics used is a two-moment rain scheme developed by Seifert and Beheng (2001) and implemented following Stevens and Seifert (2008). ED(MF)^n is included into the UCLA LES by replacing the standard SGS of the LES, whereby ED(MF)^n is only applied to the prognostic thermodynamic state variables and not to momentum. In each column of the LES, the ED(MF)^n initializes n updrafts at the surface, which continue to rise until they reach their termination height. Because of the dependence of the plume model [Eqs. (5) and (6)] on the local environment, the termination height will become dependent

on it (Brast et al. 2016). Also, the eddy diffusivity is calculated for each column [the ED part of ED(MF)^n]. For most simulations in this study, a maximum of $n = 10$ updrafts will be used, which makes its computational efficiency comparable with other convection schemes, as shown by Neggers (2015). Accordingly, the use of $n = 10$ is a reasonable compromise between resolving the size density while minimizing computational costs. In UCLA LES, the ED(MF)^n scheme with 10 plumes is also 10 times more computationally expensive compared to its default Smagorinsky scheme. This nicely illustrates the typical difference in computational cost of subgrid parameterization in an LES and a GCM. A sensitivity study of n is given in section 4c.

To study the scale adaptivity of the parameterization scheme, 10 simulations with the UCLA LES ED(MF)^n system were performed with horizontal resolutions ranging from 100 m to 1 km and a fixed vertical resolution of 40 m. Note that a simulation at 1-km resolution can no longer be called an LES, as the largest boundary layer eddies are no longer resolved. In this range, the LES framework merely acts as a nonhydrostatic circulation model, with ED(MF)^n parameterizing all the vertical transport by turbulence, while the individual columns only weakly interact laterally. Moving from low to high resolution, some thermals will become resolved, and the lateral interaction might become significant. The advantage of this framework is that this change in column interaction occurs naturally and unconstrained, because at all resolutions, the motions are nonhydrostatic.

The domains have $144 \times 144 \times 100$ grid boxes, which results in a different domain size for each simulation. This difference in domain size might affect the representation of the flow, but we speculate that this effect is negligible. The advantage of this setup is that we always have the same number of columns, which simplifies comparing the statistics of the various simulations. The 10 updrafts represent different size bins, each having a width of 100 m and together covering the range $0 < l < 1000$ m.

As a test case, the Rain in Shallow Cumulus over the Ocean (RICO) case is chosen (vanZanten et al. 2011). This case is a well-documented quasi-equilibrium case of marine shallow cumulus convection, with time-constant large-scale forcing approximately balanced by fast-acting turbulence and convection. We chose this case for our study because the absence of strong time evolution makes it easier to analyze the experiment. The LES model used in this study, UCLA LES, has participated in an intercomparison and proven to be suitable to simulate this case (Rauber et al. 2007). The simulation time was 9 h, where the last 3 h are used for analysis.

3. Parameterizations in the gray zone

Before analyzing the behavior of ED(MF)^n in the gray zone, it makes sense to first elaborate on the problem of modeling within the gray zone in general. How to deal with circulations in the gray zone is still an open question (Zhou et al. 2014; Ching et al. 2014). In principle, high-resolution LES can represent the circulations in the boundary layer (e.g., Ching et al. 2014; Maronga and Raasch 2013). However, when the resolutions get coarser, the circulations cannot be completely resolved anymore. Coarse-grained high-resolution LES can inform how these circulations should be represented in models with resolutions within the gray zone, because coarse-grained fields reflect processes at different scales that are fully integrated with each other and interact in the right physical way (Shin and Dudhia 2016). This behavior is not necessarily the case in simulations at the corresponding resolutions in the gray zone (Efstathiou and Beare 2015). From these studies, an important science question emerges: if is it possible at all to design scale-adaptive parameterizations that are capable of reproducing the behavior of coarse-grained LES. This means that the perfect parameterization will introduce realistic interactions between unresolved and resolved circulations. This is by no means an easy task, and much is still unclear about how this could be achieved.

This study aims to investigate this problem in more detail and to explore a possible way forward. To this purpose, we define three datasets derived from LES that act as starting points for interpreting the behavior of scale-adaptive models in the boundary layer gray zone, to be discussed in section 4.

The first dataset, referred to as smag, is derived from a set of simulations with the default Smagorinsky–Lilly-type scheme at a range of resolutions that spans the boundary layer gray zone and with the setup described above. This setup reflects the usual way of running LES.

The second dataset, called ED(MF)^n unf, consists of a similar set of simulations but with ED(MF)^n replacing the Smagorinsky–Lilly subgrid scheme and still without size filtering. This setup represents the behavior of a non-scale-adaptive GCM shallow cumulus scheme in the boundary layer gray zone.

The third dataset, called smag cg, consists of coarse-grained fields at various subdomain sizes within two high-resolution LES simulations with the Smagorinsky–Lilly-type scheme. The coarse graining of LES has been used by various other studies to study various grid sizes (e.g., Shutts and Palmer 2007; Honnert et al. 2011; Dorrestijn et al. 2013; Efstathiou and Beare 2015; Honnert et al. 2016). Hereby, we average the data horizontally over an area corresponding to the resolution of the

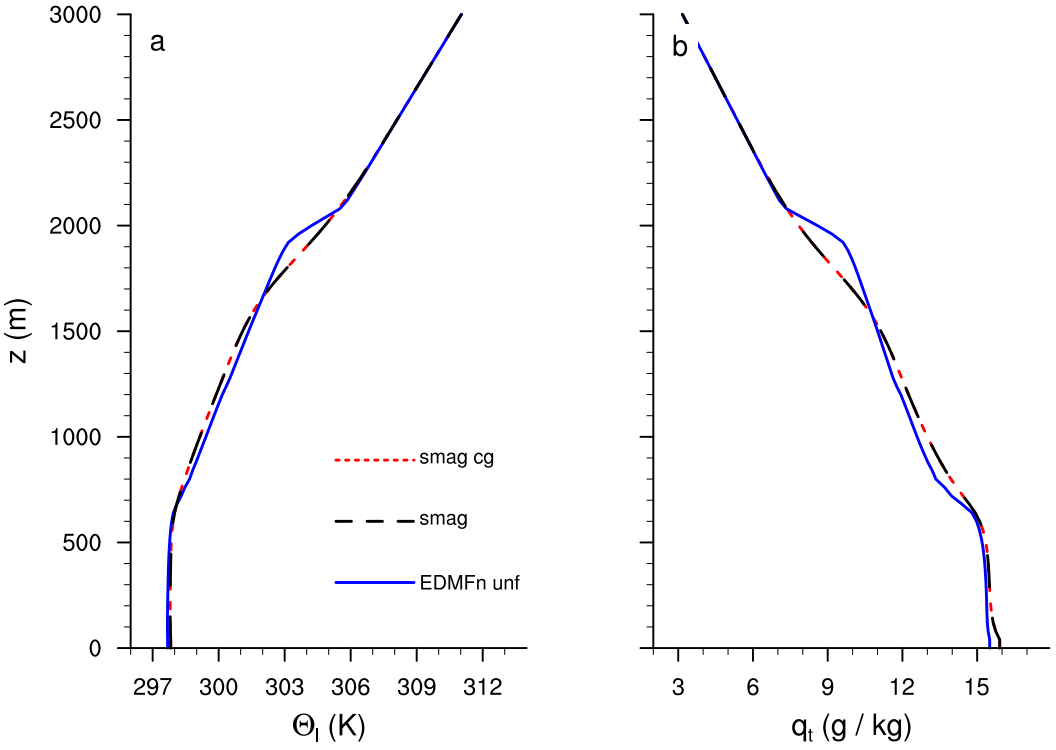

FIG. 2. Mean profiles of (a) Θ_l and (b) q_t averaged horizontally and over 3 h for smag cg, smag, and ED(MF)^n unffor a resolution of 100 m.

coarse-grained field (see Shutts and Palmer 2007). One simulation has a horizontal resolution of 100 m and a domain size of 512 × 512 grid points; the other has a resolution of 25 m and a domain size of 200 × 200 grid points. The use of two simulations is adopted to reduce the computational burden of these simulations and has previously been used by Dorrestijn et al. (2013). We adopt the working hypothesis that the smag cg dataset represents how a perfect, successful scale-adaptive parameterization should behave in the boundary layer gray zone.

The mean profiles of the thermodynamic state of the smag, smag cg, and ED(MF)^n unf simulations are shown in Fig. 2 for a resolution of 100 m. The results from smag cg are per definition the same as the results from smag because the underlying simulations are the same and the subdomain size is equal to the grid spacing of the simulation. For both smag and ED(MF)^n unf, the profiles are almost invariant across the different resolutions (not shown). For smag, the profiles are similar to those in vanZanten et al. (2011), while for ED(MF)^n unf, the inversion height is slightly overestimated. Horizontal cross sections of vertical velocity of the smag cg dataset at 400-m height are shown in Fig. 3 for various subdomain sizes. At small subdomain sizes, diagonal, elongated structures can be recognized in the vertical wind field, which disappear with increasing subdomain size. This behavior is well known from previous studies (e.g., Sakradzija et al. 2016; Beare 2014) and is reproduced here. The smag simulation behaves similarly (not shown).

Figure 4 compares the subgrid and total vertical flux of humidity for smag, smag cg, and ED(MF)^n unf. Smag cg shows a gradual transition between resolved and subgrid transport with subdomain size, with more subgrid transport for larger subdomains at all heights. For the smag simulation, the subgrid transport in the cloud layer is always small compared to the resolved part. This suggests that a default Smagorinsky–Lilly-type subgrid scheme as developed for application in high-resolution LES is not appropriate for these resolutions. Similar behavior has been found by Cheng et al. (2010). The ED(MF)^n unf simulation is far too active in the subgrid transport, so all transport is subgrid and no transport is resolved even for coarse resolutions. The ratio of the subgrid transport to the total transport, as averaged over the depth of the cumulus cloud layer, in shown in Fig. 5. For ED(MF)^n unf, the subgrid dominates the total transport, while for smag, the resolved transport always dominates. Only for smag cg, a change from resolved transport at high resolutions to subgrid transport at coarse resolutions occurs. This S shape has been found in other studies (Dorrestijn et al. 2013; Honnert et al. 2016).

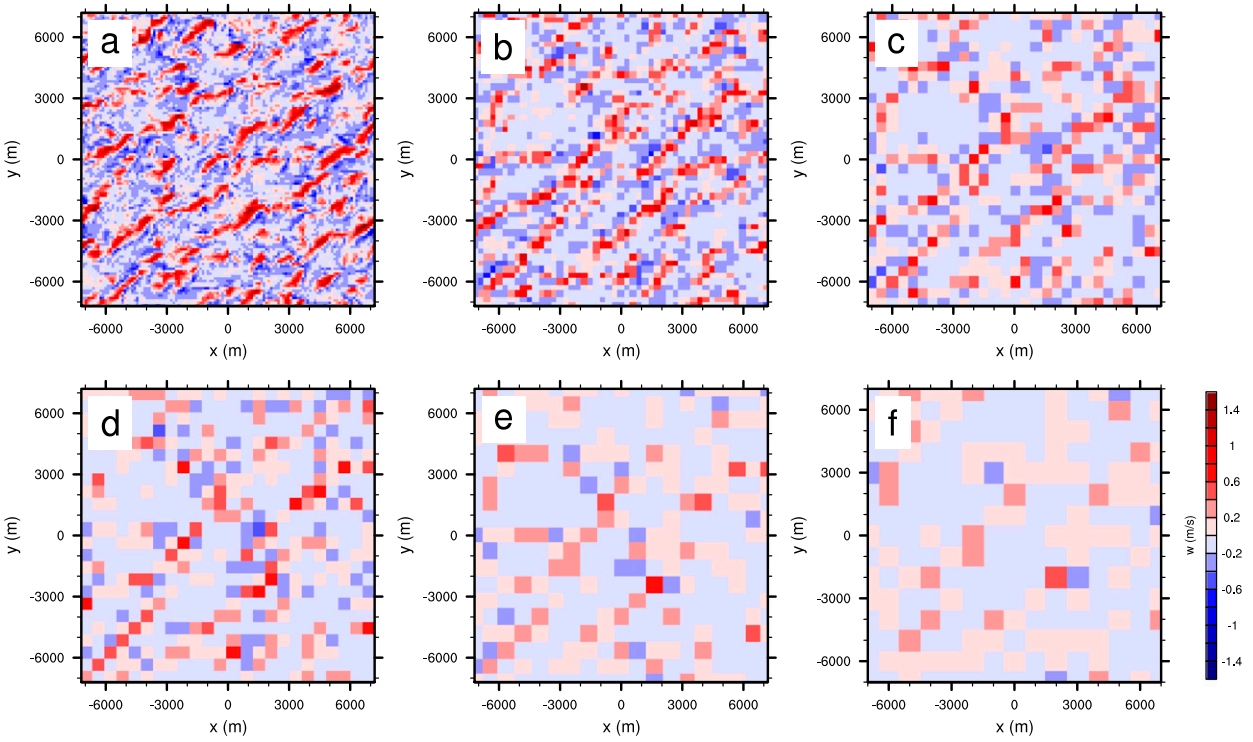

FIG. 3. Horizontal cross sections of vertical velocity at a height of 400 m after 9 h for smag cg for simulations with resolutions of (a)–(f) 100, 300, 500, 600, 800, and 1000 m.

What these results suggest is that both the default LES setup (i.e., smag) and the GCM setup [i.e., ED(MF)^n unf] fail to reproduce a subgrid contribution that gradually reduces with increasing resolution. The smag cg results represent the behavior that a scale-adaptive parameterization of vertical transport should have in the gray zone if it is interactive with the resolved flow in the correct way. We aim to reproduce the changing partitioning between subgrid and resolved contributions across the gray zone while at the same time preserving the amplitude and vertical structure of the thermodynamic state, clouds, and transport. Previous studies have captured this partitioning for turbulence schemes (e.g., Cheng and Xu 2008; Cheng et al. 2010). In this study, a first step toward such a scale-adaptive scheme for advective mass flux transport that is applicable to shallow cumulus convection is made by implementing the spectral ED(MF)^n into LES and applying size filtering in its size distribution. The behavior of this setup is discussed in the next section.

4. Behavior of ED(MF)^n

At different resolutions, the ability of the LES to resolve shallow cumulus clouds varies. A certain cloud can be resolved at fine resolutions, while it becomes a subgrid-scale process at coarser resolutions. How the ED(MF)^n subgrid scheme responds to these resolution changes, and how its activity depends on it, is studied in detail in the next sections.

a. *ED(MF)^n behavior*

The thermodynamic profiles of ED(MF)^n are shown in Fig. 6 for different resolutions. The profiles are similar to the profiles from smag except for the coarser resolutions where the boundary layer height increases slightly, which could be due to the fact that the entrainment decreases with increasing plume size. The horizontal cross sections of vertical velocity (Fig. 7) show a similar behavior as in smag cg. The magnitude of the velocity decreases slightly faster toward coarser resolutions. Also shown are the outlines of the clouds resolved by LES, which are located above the updrafts in the subcloud layer. For the simulation with a fine resolution of 100 m, most clouds are resolved, while almost no clouds are resolved for grid sizes of 800 m and more.

Figures 8 and 9 show profiles of different variables at a range of LES resolutions, decomposed into contributions by ED(MF)^n, by the LES, and by ED(MF)^n and LES together. In Figs. 8c and 8f, the total transport is more or less the same at all resolutions. At first thought, one might expect this behavior, as the instability created

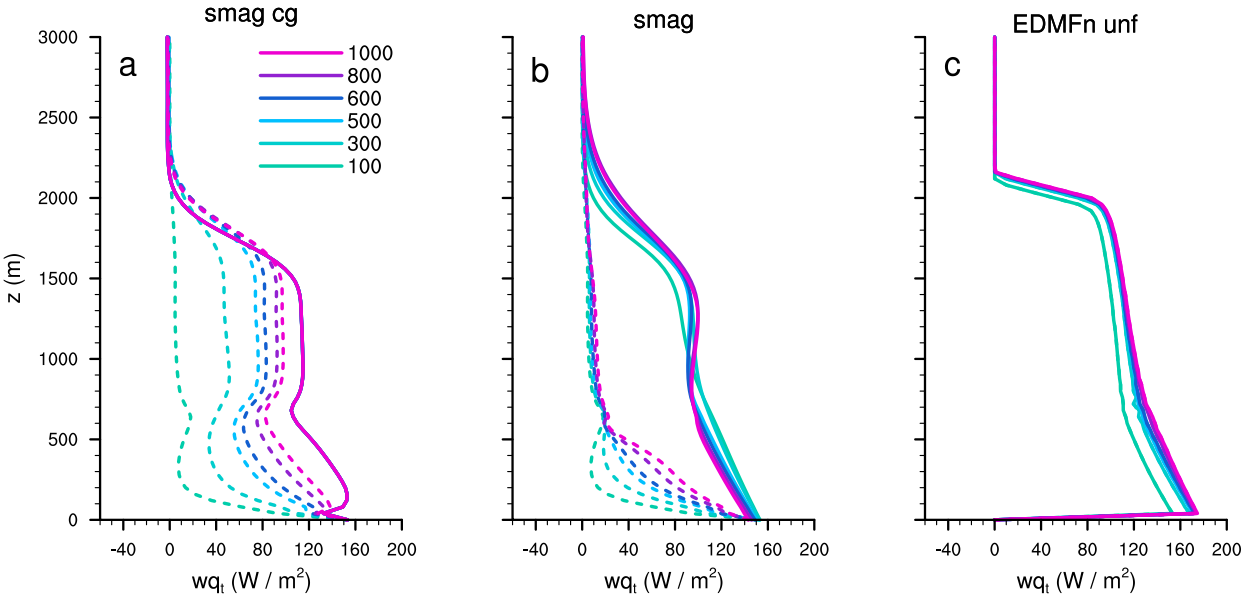

FIG. 4. Profiles of vertical transport of q_t averaged horizontally and over 3 h at different resolutions (in colors) for (a) smag cg, (b) smag, and (c) ED(MF)^n unf. Dashed lines represent the subgrid contribution of the transport, while solid lines show the total transport.

by the prescribed large-scale forcing is the same for all experiments; however, many SCM intercomparison studies (e.g., Lenderink et al. 2004) have shown that convective parameterizations can vary greatly in activity given a certain instability. In other words, the robustness of the transport profiles across this range of resolutions is not trivial. It has to be mentioned that the boundary layer does not develop in exactly the same way in all simulations (i.e., some resolution dependency exists). At coarser resolutions, the boundary layer deepens quicker, which was already seen in the thermodynamic profiles. Near the surface, the peaks of the fluxes differ slightly, probably because the resolution near the ground at the coarse resolutions is not sufficient to resolve these peaks. The covariance of heat and moisture shows that at fine resolutions, the LES contributes most of the transport, while at coarse resolutions, ED(MF)^n takes over.

The same behavior shown in Fig. 8 is evident for some cloud variables (Figs. 9c,f,i) in that the vertical structure and the magnitude of the cloud fraction, cloud condensate, and cloud mass flux profiles are reasonably robust. For cloud fraction and condensate, discretized steps of the cloud variables appear at coarse resolutions, which is dependent on the number of rising plumes. Only the largest plumes represent the clouds, so when using 10 plumes, only about two plumes represent most of the transport, and when one plume stops, a step in the cloud variable appears. The impact of the number of plumes is further studied in section 4c.

While the apparent robustness of total transport and clouds is encouraging, much more intriguing is the shift in the partitioning between parameterized and resolved flux that takes place across the gray zone. This behavior is far from trivial, and it shows that the size-filtered ED(MF)^n is indeed scale adaptive. The transport of heat and moisture is achieved almost exclusively by the LES at the fine resolutions, while at the coarse resolutions,

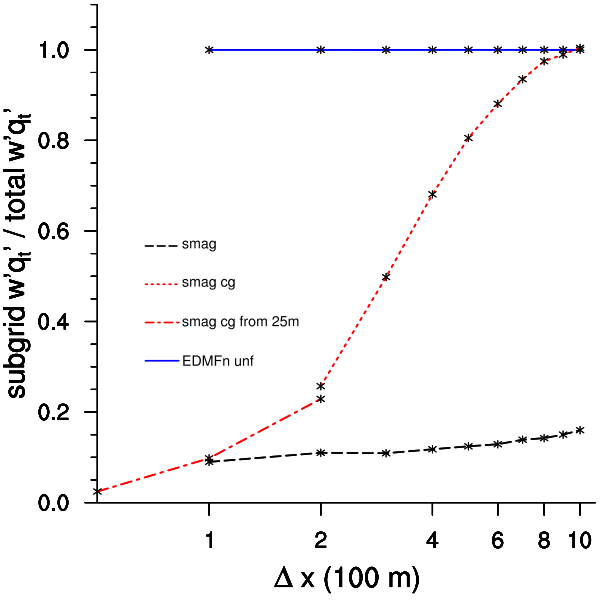

FIG. 5. Ratio between subgrid and resolved flux of q_t averaged horizontally, over 3 h, and over the heights between 400 and 2000 m for smag, smag cg, and ED(MF)^n unf; smag is extended to finer resolutions with results from smag cg with a resolution of 25 m.

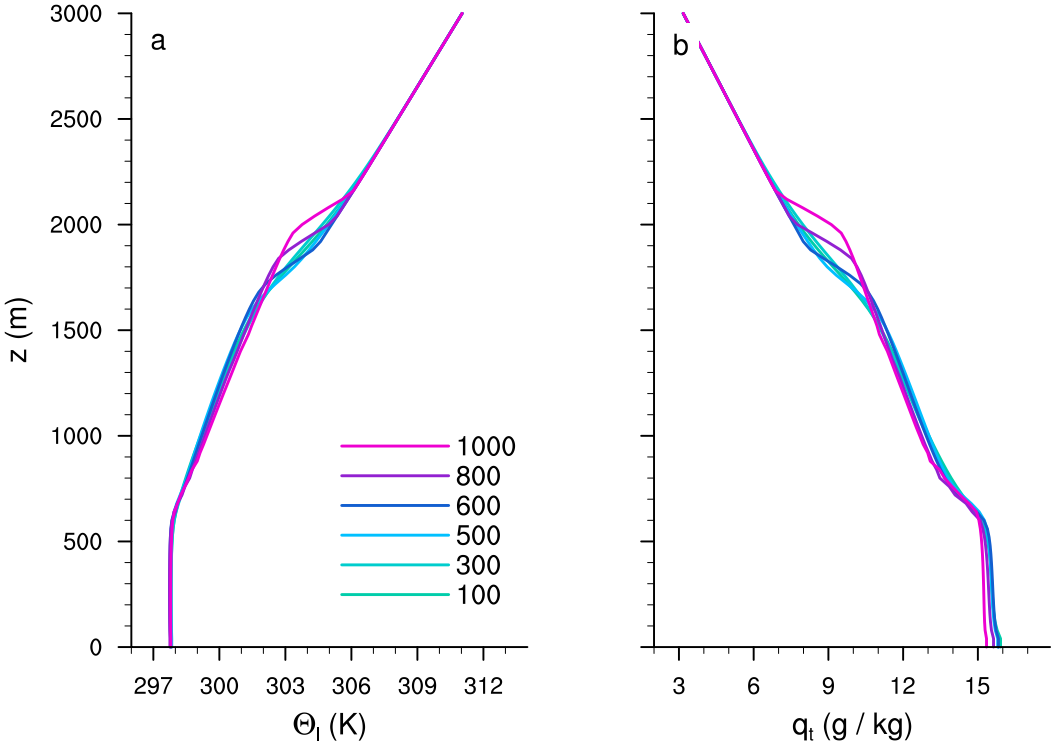

FIG. 6. Mean profiles of (a) Θ_l and (b) q_t averaged horizontally and over 3 h for the size-filtered ED(MF)^n simulations for different resolutions indicated by the colors.

the subgrid scheme, which is in our case the ED(MF)^n parameterization scheme, takes over the transport. This behavior is similar to the results from the coarse-grained simulations (Fig. 4).

It is informative to investigate how the plumes of ED(MF)^n and the clouds of the LES interact (Brast et al. 2016). To this purpose, a comparison was made between LES cloud top and the termination height of the plumes, even though at coarse resolutions, there are no resolved clouds present in the LES. Figure 10 shows this comparison for the simulations with resolutions of 100 to 600 m. Only these finer resolutions were taken to illustrate the comparison of the termination heights of the plumes with the LES clouds, because at coarser resolution, the LES resolves hardly any clouds. At fine resolutions, the termination height of most plumes is close to the LES cloud tops, and the upper triangle of the plot is almost empty, because the parameterized plumes stop at low heights and most of the cumulus clouds are resolved by the LES (see Fig. 7, resolution 100 m). The dots on the diagonal line denote those plumes that are rising within a resolved LES cloud and thus reach the same termination height as the LES clouds (Brast et al. 2016). With decreasing resolutions (Fig. 10b), the plume-termination height increases compared to the LES cloud-top height. Here, less clouds are resolved and the plumes pick up the subgrid transport and therefore rise higher. The LES clouds that are still resolved at these coarser resolutions are shallow. This is a further indicator that the cloud representation shifts from the LES to the ED(MF)^n with decreasing resolution.

At all resolutions, the ratio between subgrid and resolved flux of q_t was calculated by averaging over the horizontal domain, over 3 h, and over the heights between 400 and 2000 m (Fig. 11, black line), resulting in an S plot similar to Fig. 2 in Dorrestijn et al. (2013) and Fig. 2 in Honnert et al. (2016) and also similar to the coarse-grained results (Fig. 5). This illustrates that the shift in representation of the cumulus clouds from low to high resolutions happens in a gradual way. This partitioning has not been prescribed as a function of resolution but is achieved by the scheme itself through the size filtering of the discretized size densities. Different height averaging gives the same results as long as the height interval roughly covers the cloud layer, which is shown in Fig. 11a. Here, the ratio is studied at certain heights corresponding to the mixed layer and the cloud layer. It can be seen that the distribution between resolved and subgrid fluxes behaves scale adaptively in the mixed layer (at 400 m) as well as in the cloud layer (at 1000 m). Especially in the mixed layer, the ratio is similar to smag cg. In the subcloud layer, the mass flux part of

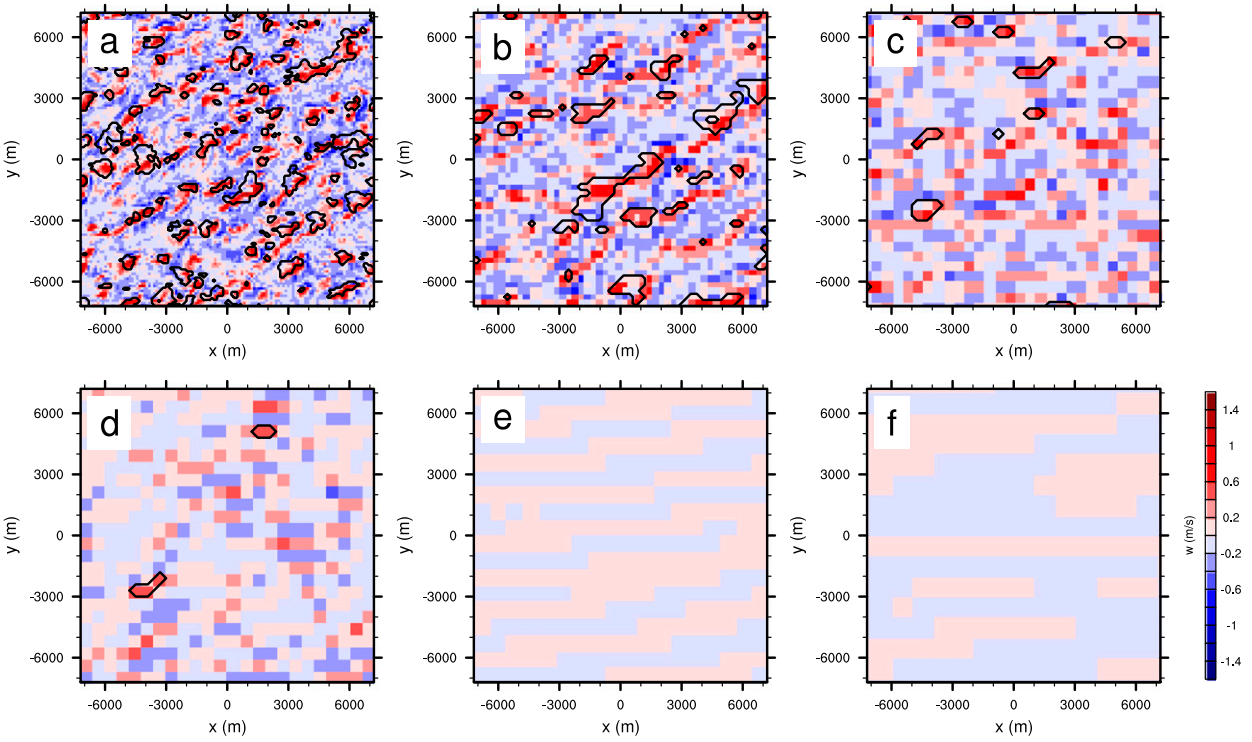

FIG. 7. As in Fig. 3, but for ED(MF)^n simulations. The black lines show the outline of the clouds resolved by LES.

the flux seems to be smaller, but as soon as the resolution is coarse enough to include big plumes in the ensemble, the mass flux increases in the cloud layer. Figure 11b shows the standard deviation of the subgrid flux, which represents the variability between the ED(MF)^n transport conducted in all columns. A maximum of the standard deviation implies that in this range of resolutions, the subgrid scheme is very responsive to the local environment. It exhibits a peak in the gray zone, representing the transition between clouds being mostly parameterized at coarse resolutions and clouds being mostly resolved at fine resolutions. The location and the magnitude of this peak are in accordance with those in Dorrestijn et al. (2013). At fine resolutions, there is an increase in the standard deviation, which mainly originates from the middle of the cloud layer (not shown).

b. *Energy spectra*

Although it is important that the size-filtered ED(MF)^n is able to adapt its transport activity to fit the resolution while still maintaining the total transport, the energy of the flow should also be well represented across the gray zone for scales unresolved by the LES. To investigate in more detail how much energy is represented by the different scales, we analyzed the spectrum of the LES at different resolutions. Previous studies have shown that the power spectrum of vertical velocity is dependent on resolution (Sakradzija et al. 2016). Therefore, to avoid this possible problem, we use the smag cg simulation at resolution 100 m to act as an additional reference. This simulation is the basis for the coarse-grained simulations but is not coarse grained yet at 100-m resolution. We use this simulation as reference because the domain is larger than for smag. Using this reference should help interpret the power spectra diagnosed from the UCLA LES ED(MF)^n runs at various resolutions. With decreasing resolution, the energy of the scales smaller than the grid size should become more and more represented by the ED(MF)^n. To calculate the energy of ED(MF)^n, the energy for every group of plumes was calculated as follows:

$$E^{\mathrm{SGS}}(l,z) = \mathscr{A}(l,z)\Delta x[w(l,z) - w_{\mathrm{LES}}(z)]^2, \quad (15)$$

with E the energy, Δx the grid box length, $w(l, z)$ the vertical velocity of the individual updraft, and w_{LES} the vertical velocity of the LES. Here, the vertical velocity variance is weighted with the area fraction of the updraft $\mathscr{A}$ and the grid box size to yield the relative contribution of each size bin to the total spectrum. Note that the contribution by diffusion is not accounted for in Eq. (15), which might lead to a small underestimation of the energy when comparing to the spectra derived from LES.

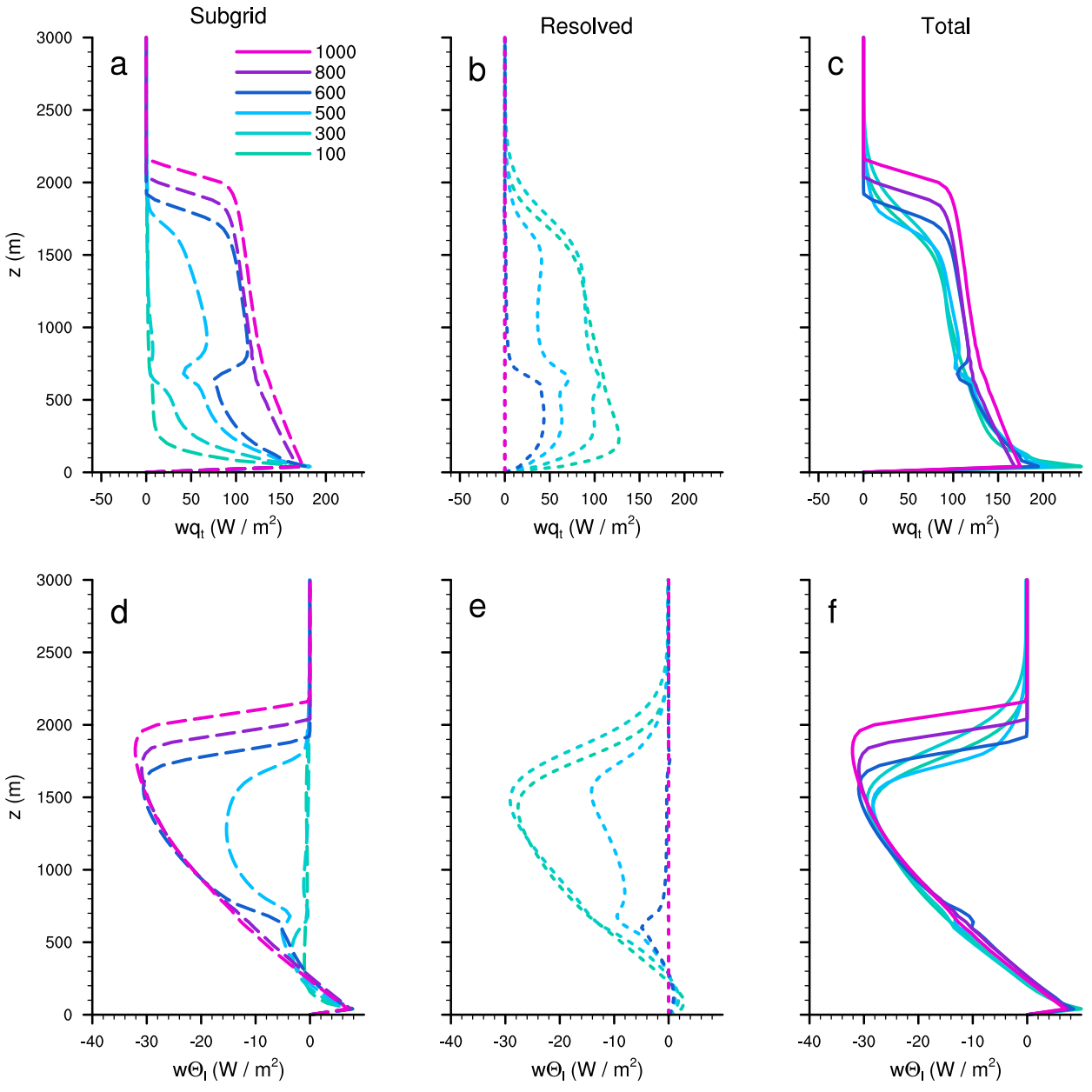

FIG. 8. Profiles of vertical transport of (a)–(c) q_t and (d)–(f) Θ_l averaged horizontally and over 3 h at different resolutions (in colors): (a),(d) dashed line is subgrid transport by ED(MF)^n; (b),(e) dotted line is resolved transport by LES; and (c),(f) solid line is total transport.

Figure 12 shows the spectra of the set of LES realizations at various resolutions. The reference LES with a larger domain size at 100-m resolution (smag cg) is always shown for reference, since this line should ideally be reproduced by the combination of LES and ED(MF)^n for all resolutions. The energy carried by the ED(MF)^n size bins is indicated by the red dots. In the ED(MF)^n simulations, the resolved part of the spectrum (black) has the typical shape of the spectra at the resolutions up to 600 m (e.g., De Roode et al. 2004), while for the coarser resolutions of 800 and 1000 m, the resolved part shows far too little energy. We think that this indicates a total collapse of the resolved turbulence, a situation in which all transport is conducted by ED(MF)^n. This is reflected by the flat w fields as shown in the last two panels of Fig. 7 and also by the profiles in Fig. 8. At high resolutions, the difference between the reference LES and the ED(MF)^n LES is very small. With decreasing

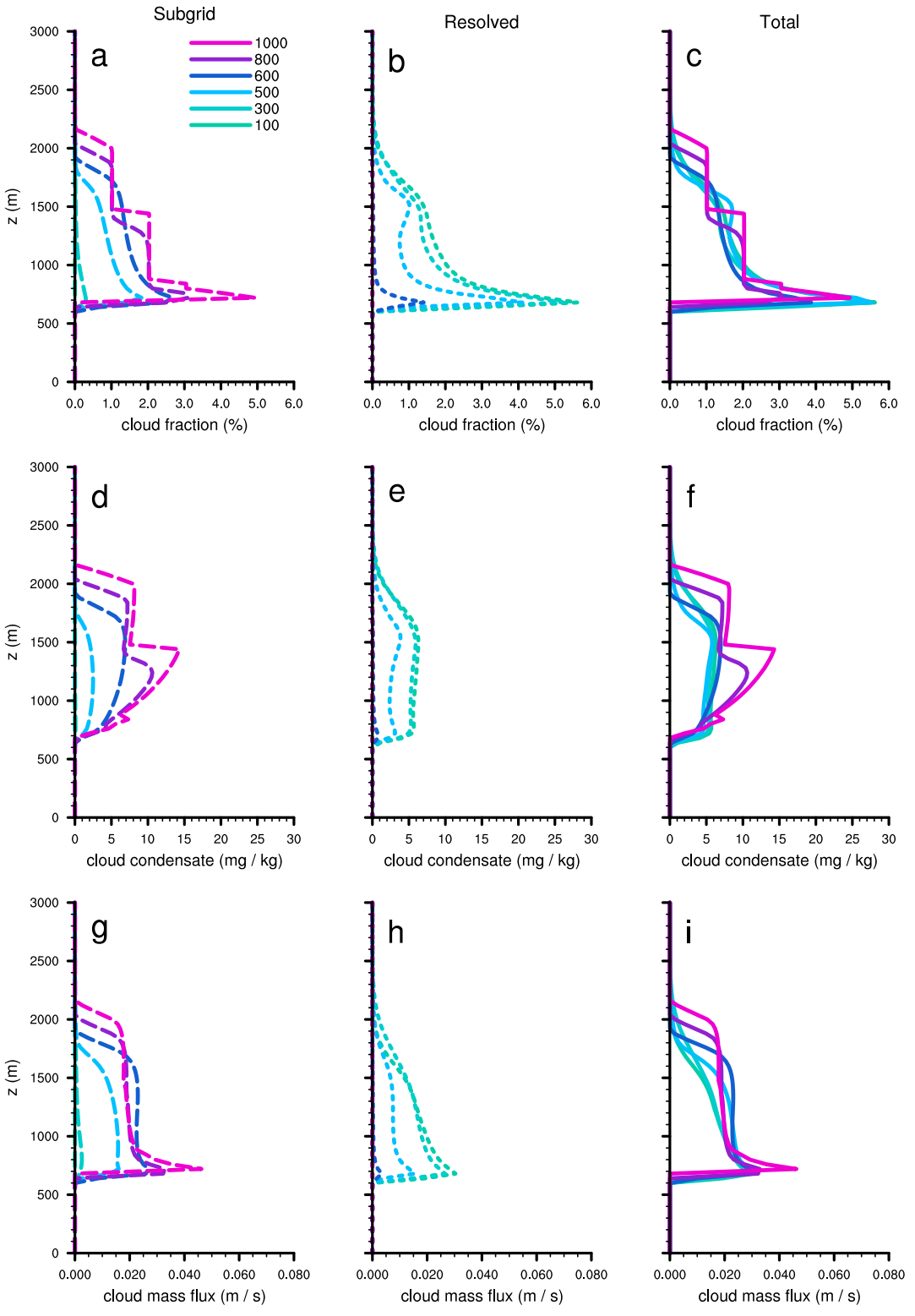

FIG. 9. Profiles of (a)–(c) cloud fraction, (d)–(f) cloud condensate, and (g)–(i) cloud mass flux averaged horizontally and over 3 h at different resolutions (in colors); (a),(d),(g) dashed line is subgrid portion by ED(MF)^n; (b),(e),(h) dotted line is resolved portion by LES; and (c),(f),(i) solid line is total profile.

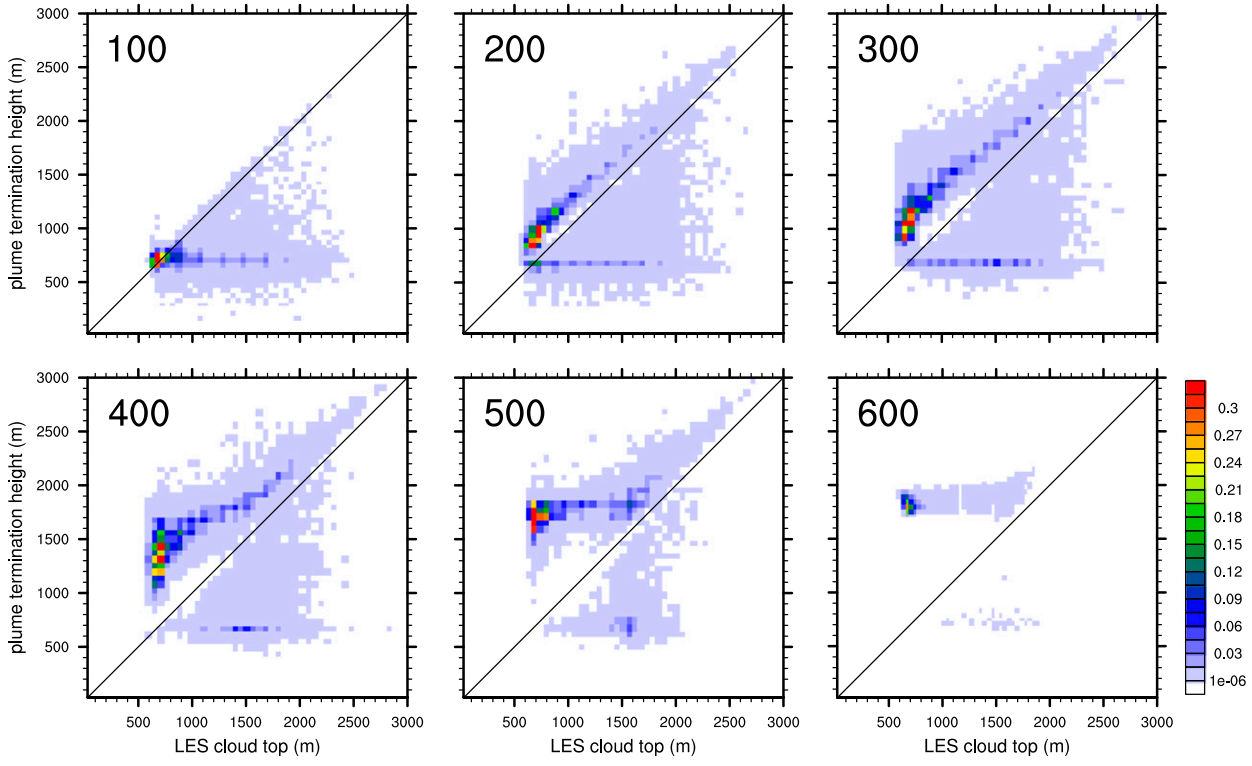

FIG. 10. Frequency density function of LES cloud-top and plume-termination height averaged over 3 h and for simulations with resolutions of 100, 200, 300, 400, 500, and 600 m.

resolution, the number of size bins in the histogram that survive the size filter and are retained in ED(MF)^n increases. The larger the updrafts are, the more energy they represent (note that in the last two panels, the 100-m updrafts contain too little energy to be plottable). The energy of the reference LES and the ED(MF)^n updrafts are similar in magnitude, and the gradient of the slope of the reference LES and the updrafts is very similar, which we take as an encouraging result. The ED(MF)^n updrafts complement the resolved spectra of

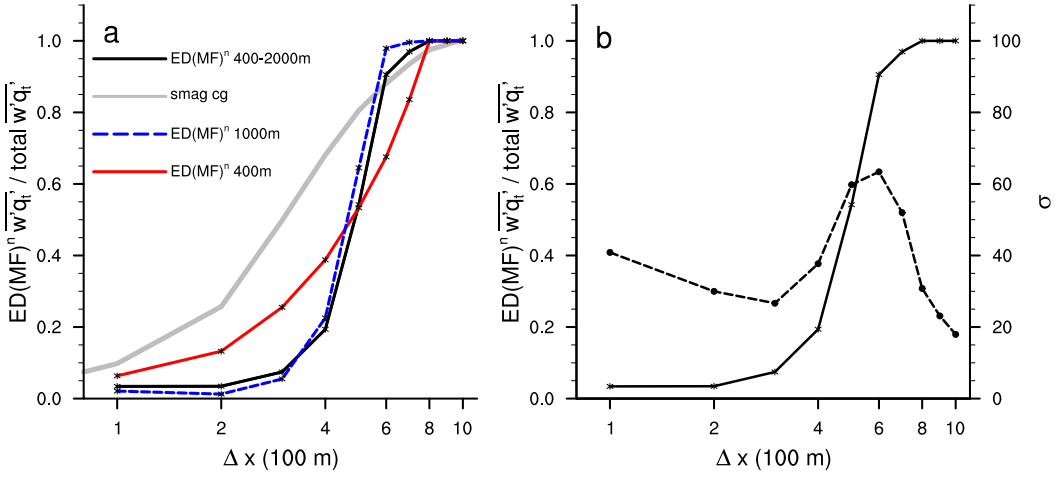

FIG. 11. Ratio between subgrid and resolved flux of q_t of the size-filtered ED(MF)^n scheme, averaged horizontally, over the heights between 400 and 2000 m and over 3 h (black line): (a) with the ratio for smag cg (gray line) and the average at height levels 400 and 1000 m (colors) and (b) with standard deviation of subgrid flux (dashed line).

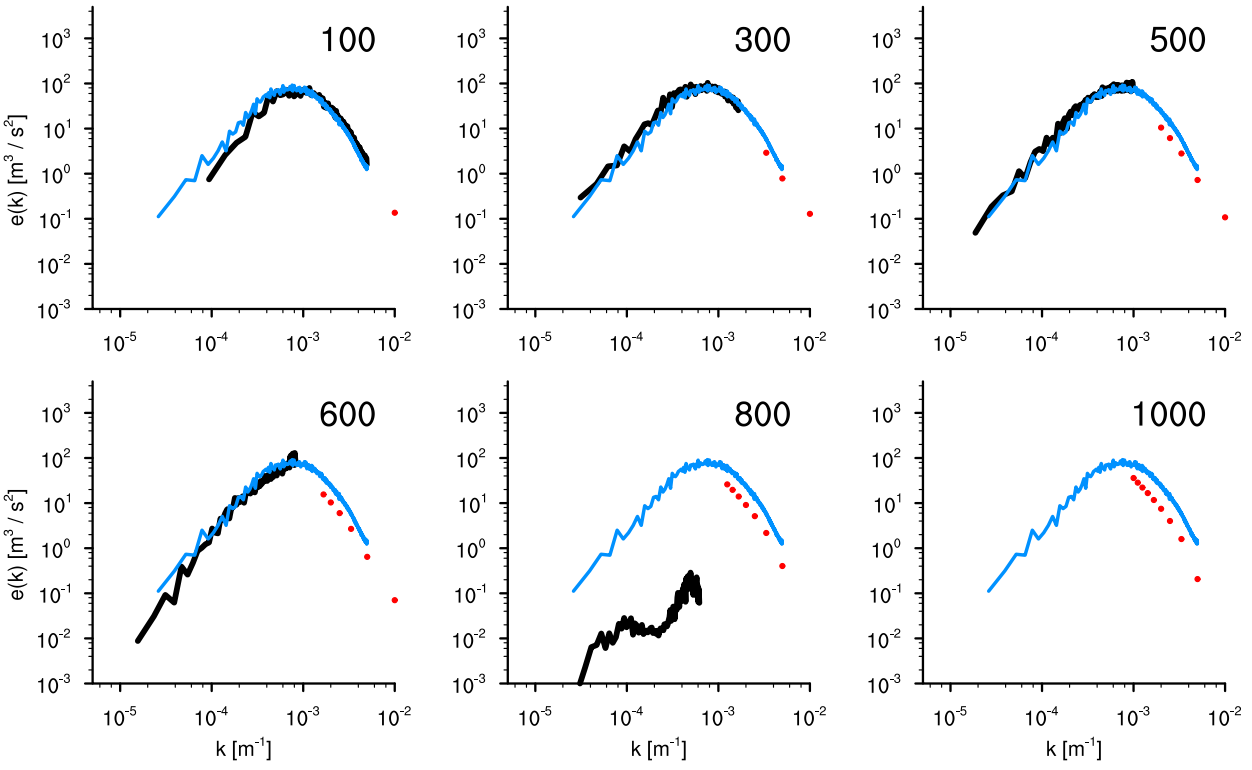

FIG. 12. Spectral energy density e of LES (lines) and ED(MF)^n (dots) at a height of 400 m averaged over 3 h for simulations with resolutions of 100, 300, 500, 600, 800, and 1000 m: black line is energy spectra of the ED(MF)^n LES with varying domain size and resolutions; blue line is the reference LES with domain size of 512 × 512 grid points and a resolution of 100 m.

the LES quite nicely, so we conclude that a gradual increase in the contribution by ED(MF)^n with decreasing resolution is also apparent in the power spectrum, such that its shape over the whole range of sizes remains roughly unaltered.

c. *Sensitivity studies*

In this section, the sensitivity of the results on some choices regarding the setup is tested to gain more insight into the behavior of ED(MF)^n. The simulations used are listed in Table 1. All of these simulations have a smaller domain size to save computing time, which affects the results only negligibly (not shown).

The first sensitivity study considers the impact of introducing the scale adaptivity of the eddy diffusivity by using an ED component without the scale-dependent adjustments as discussed in section 2c (noED). The second sensitivity test addresses the impact of the number of bins in the discretized size density by using 50 updrafts instead of 10, which are evenly distributed in size between 0 and 1000 m (50up). As before, the size bins larger than the grid spacing are still filtered out. The third test assesses the impact of the total area fraction a covered by the updrafts [Eq. (4)]. In the reference simulation (ref), this fraction has a constant value of 10%. Now we run two sets of simulations with constant values of 5% (a5) and 20% (a20).

The impact on the ratio of the subgrid to the total humidity transport across resolutions is shown in Fig. 13. Simulation noED is similar to the reference simulation but overrepresents the subgrid transport at fine resolutions, indicating that the adjustment made to the scale adaptivity of the eddy diffusivity is necessary for ED(MF)^n to be truly scale adaptive. Simulation 50up shows that the results are not very sensitive to the number of updrafts. Ten updrafts seem to be enough to represent the subgrid transport and indicate a good compromise between a detailed representation of different cloud sizes and computing cost. An advantage of using 50 updrafts is that the discretized steps in the reference simulation seen in Fig. 9 are smoothed out (not shown), because most of the transport is done by the largest updrafts, and in this simulation, there is a larger number of large updrafts. For simulation a20, the gray zone (i.e., the transition between the clouds being parameterized and resolved) is shifted toward finer resolutions. At the coarse resolution, no change occurs with respect to the reference simulation, because the

TABLE 1. Overview over sensitivity studies.

	Horizontal domain size in grid points	Scale-adaptive ED	No. of updrafts	Updraft fraction a
ref	144 × 144	Yes	10	10%
noED	96 × 96	No	10	10%
50up	96 × 96	Yes	50	10%
a5	96 × 96	Yes	10	5%
a20	96 × 96	Yes	10	20%

distribution of the updrafts is similar and all transport is done by the subgrid scales. At the fine resolutions, almost all transport is resolved, which also results in a small difference between simulations and a20. Only at the midresolutions, a change is apparent. The same explanation holds for simulation a5, where the behavior goes in the other direction, with the transport smaller at the midresolutions. Apparently, the size filtering is crucial for letting the system obtain a realistic S shape in the resolution dependence of the ratio of SGS to total flux.

5. Summary and conclusions

This study discusses a first step toward scale-adaptive advective flux modeling by size filtering a cloud-size–density-based mass flux scheme for shallow cumulus convection. To this purpose, the ED(MF)^n scheme was implemented into an LES as an SGS scheme. Size filtering was applied to the spectral mass flux component that is coupled to the horizontal resolution. This setup was then run at various resolutions and compared to coarse-grained results from LES, since we adopt as our working hypothesis that a perfect scale-adaptive parameterization scheme should reproduce the behavior of a coarse-grained LES in the gray zone. The advantages of using LES in this manner is that it acts as a simple and transparent circulation model while still retaining nonhydrostatic effects. This makes the interpretation of the results easier. We argue that this system can effectively act as an interactive testing ground for scale-adaptive parameterizations.

We find that applying size filtering to the ED(MF)^n scheme does indeed introduce scale adaptivity that is similar to that observed in offline subdomain analyses of LES fields as reported by previous studies (e.g., Dorrestijn et al. 2013; Shin and Dudhia 2016), and which is similar to results from turbulence schemes (Cheng and Xu 2008; Cheng et al. 2010). This size filtering is key to reproduce the typical S-shaped curve in the resolution dependence of the relative SGS activity, which has been presented here for a coarse-grained LES (smag cg). The gradual transition from subgrid to resolved was also apparent in the reconstructed power spectrum.

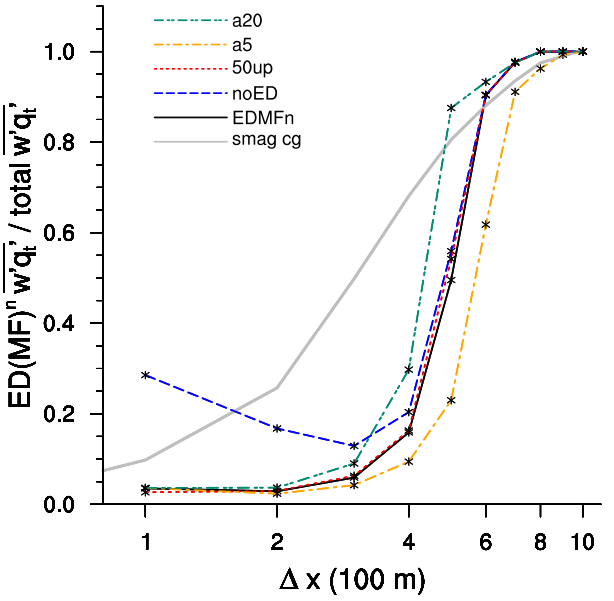

FIG. 13. Ratio between subgrid and total flux of q_t, averaged over 3 h and averaged over the height range 400–2000 m. The colors indicate the results of the different sensitivity studies as indicated in the legend (see text).

The scheme studied here is scale adaptive mostly because of the size filtering in the spectral mass flux component. Note however that to make the scheme work satisfactorily as a whole, the ED part of the scheme was made scale adaptive as well by adapting the K_h parameter. Without this adaptation, the scheme conducts excessive eddy diffusivity transport at fine resolutions. This shows that for a true scale adaptivity, the ED part of ED(MF)^n must also be scale aware. Further sensitivity studies showed that a higher number of updrafts does not fundamentally change the results, while changing the constant total area fraction of the updrafts leads to a modest shift in the gray zone.

Several simplifications were made regarding the design of ED(MF)^n concerning the shape of the size distribution and the representation of stochastic effects due to subsampling of the plume population. These topics are subject to ongoing research. This scheme is designed for surface-driven regimes such as shallow cumulus clouds but could in principle also be used for deep convection (Neggers 2015). This would require upgrades (i) in the microphysics module in the plume model, (ii) in the option to represent transport by downdrafts, and (iii) to account for the impact of spatial organization on vertical transport. For other regimes such as stratocumulus, which are not surface driven, the scheme would need to be adapted so that the plumes are not initialized at the surface. Nevertheless, despite its primitive design, the tests with the scheme as an SGS scheme inside an LES do

demonstrate its scale adaptivity, and our results highlight the potential of spectral schemes in scale-adaptive modeling in general. Finally, the impact of this skill on the larger-scale flow in the gray zone of convection still needs to be explored, for example, by implementation into a GCM and performing global simulations. This is also a future research topic.

Acknowledgments. This project was funded by the Helmholtz Association in the framework of the Helmholtz Water Network and by Grant GSGS-2017A-F02 of the Graduate School of Geosciences, University of Cologne, to M.B. The lead author was supported by the Energy Transition and Climate Change (ET-CC) excellence initiative of the University of Cologne. Parts of the simulations were run on CHEOPS, the cluster of the Regionales Rechenzentrum of the University of Cologne. The authors also gratefully acknowledge the computing time granted by the John von Neumann Institute for Computing (NIC) and provided on the supercomputer JURECA at Jülich Supercomputing Centre (JSC; Jülich Supercomputing Centre 2016). Parts of this work have been previously presented at the EGU 2017, the UCP 2016, and the AGU 2015. The data used in this study can be obtained from the corresponding author upon request.

REFERENCES

Angevine, W. M., H. Jiang, and T. Mauritsen, 2010: Performance of an eddy diffusivity–mass flux scheme for shallow cumulus boundary layers. *Mon. Wea. Rev.*, **138**, 2895–2912, https://doi.org/10.1175/2010MWR3142.1.

Arakawa, A., 2004: The cumulus parameterization problem: Past, present, and future. *J. Climate*, **17**, 2493–2525, https://doi.org/10.1175/1520-0442(2004)017<2493:RATCPP>2.0.CO;2.

——, and W. H. Schubert, 1974: Interaction of a cumulus cloud ensemble with the large-scale environment, part I. *J. Atmos. Sci.*, **31**, 674–701, https://doi.org/10.1175/1520-0469(1974)031<0674:IOACCE>2.0.CO;2.

——, J.-H. Jung, and C.-M. Wu, 2011: Toward unification of the multiscale modeling of the atmosphere. *Atmos. Chem. Phys.*, **11**, 3731–3742, https://doi.org/10.5194/acp-11-3731-2011.

Beare, R. J., 2014: A length scale defining partially-resolved boundary-layer turbulence simulations. *Bound.-Layer Meteor.*, **151**, 39–55, https://doi.org/10.1007/s10546-013-9881-3.

Betts, A. K., 1973: Non-precipitating cumulus convection and its parameterization. *Quart. J. Roy. Meteor. Soc.*, **99**, 178–196, https://doi.org/10.1002/qj.49709941915.

Bhattacharya, R., and B. Stevens, 2016: A two turbulence kinetic energy model as a scale-adaptive approach to modeling the planetary boundary layer. *J. Adv. Model. Earth Syst.*, **8**, 224–243, https://doi.org/10.1002/2015MS000548.

Bogenschutz, P. A., and S. K. Krueger, 2013: A simplified PDF parameterization of subgrid-scale clouds and turbulence for cloud-resolving models. *J. Adv. Model. Earth Syst.*, **5**, 195–211, https://doi.org/10.1002/jame.20018.

Böing, S. J., H. J. J. Jonker, A. P. Siebesma, and W. W. Grabowski, 2012: Influence of the subcloud layer on the development of a deep convective ensemble. *J. Atmos. Sci.*, **69**, 2682–2698, https://doi.org/10.1175/JAS-D-11-0317.1.

Boutle, I. A., J. E. J. Eyre, and A. P. Lock, 2014: Seamless stratocumulus simulation across the turbulent gray zone. *Mon. Wea. Rev.*, **142**, 1655–1668, https://doi.org/10.1175/MWR-D-13-00229.1.

Brast, M., R. A. J. Neggers, and T. Heus, 2016: What determines the fate of rising parcels in a heterogeneous environment? *J. Adv. Model. Earth Syst.*, **8**, 1674–1690, https://doi.org/10.1002/2016MS000750.

Cheng, A., and K.-M. Xu, 2008: Simulation of boundary-layer cumulus and stratocumulus clouds using a cloud-resolving model with low- and third-order turbulence closures. *J. Meteor. Soc. Japan*, **86A**, 67–86, https://doi.org/10.2151/jmsj.86A.67.

——, ——, and B. Stevens, 2010: Effects of resolution on the simulation of boundary-layer clouds and the partition of kinetic energy to subgrid scales. *J. Adv. Model. Earth Syst.*, **2** (3), https://doi.org/10.3894/JAMES.2010.2.3.

Ching, J., R. Rotunno, M. LeMone, A. Martilli, B. Kosovic, P. A. Jimenez, and J. Dudhia, 2014: Convectively induced secondary circulations in fine-grid mesoscale numerical weather prediction models. *Mon. Wea. Rev.*, **142**, 3284–3302, https://doi.org/10.1175/MWR-D-13-00318.1.

Dawe, J. T., and P. H. Austin, 2012: Statistical analysis of an LES shallow cumulus cloud ensemble using a cloud tracking algorithm. *Atmos. Chem. Phys.*, **12**, 1101–1119, https://doi.org/10.5194/acp-12-1101-2012.

De Roode, S. R., P. G. Duynkerke, and H. J. J. Jonker, 2004: Large-eddy simulation: How large is large enough? *J. Atmos. Sci.*, **61**, 403–421, https://doi.org/10.1175/1520-0469(2004)061<0403:LSHLIL>2.0.CO;2.

Dorrestijn, J., D. T. Crommelin, A. P. Siebesma, and H. J. J. Jonker, 2013: Stochastic parameterization of shallow cumulus convection estimated from high-resolution model data. *Theor. Comput. Fluid Dyn.*, **27**, 133–148, https://doi.org/10.1007/s00162-012-0281-y.

Efstathiou, G. A., and R. J. Beare, 2015: Quantifying and improving sub-grid diffusion in the boundary-layer grey zone. *Quart. J. Roy. Meteor. Soc.*, **141**, 3006–3017, https://doi.org/10.1002/qj.2585.

Fritsch, J. M., and C. F. Chappell, 1980: Numerical prediction of convectively driven mesoscale pressure systems. Part I: Convective parameterization. *J. Atmos. Sci.*, **37**, 1722–1733, https://doi.org/10.1175/1520-0469(1980)037<1722:NPOCDM>2.0.CO;2.

Grant, A. L. M., 2001: Cloud-base fluxes in the cumulus-capped boundary layer. *Quart. J. Roy. Meteor. Soc.*, **127**, 407–421, https://doi.org/10.1002/qj.49712757209.

Heus, T., and Coauthors, 2010: Formulation of the Dutch Atmospheric Large-Eddy Simulation (DALES) and overview of its applications. *Geosci. Model Dev.*, **3**, 415–444, https://doi.org/10.5194/gmd-3-415-2010.

Honnert, R., V. Masson, and F. Couvreux, 2011: A diagnostic for evaluating the representation of turbulence in atmospheric models at the kilometric scale. *J. Atmos. Sci.*, **68**, 3112–3131, https://doi.org/10.1175/JAS-D-11-061.1.

——, F. Couvreux, V. Masson, and D. Lancz, 2016: Sampling the structure of convective turbulence and implications for grey-zone parametrizations. *Bound.-Layer Meteor.*, **160**, 133–156, https://doi.org/10.1007/s10546-016-0130-4.

Jülich Supercomputing Centre, 2016: JURECA: General-purpose supercomputer at Jülich Supercomputing Centre. *J. Large-Scale Res. Facil.*, **2**, A62, https://doi.org/10.17815/jlsrf-2-121.

Kain, J. S., and J. M. Fritsch, 1990: A one-dimensional entraining/detraining plume model and its application in convective parameterization. *J. Atmos. Sci.*, **47**, 2784–2802, https://doi.org/10.1175/1520-0469(1990)047<2784:AODEPM>2.0.CO;2.

Lenderink, G., and Coauthors, 2004: The diurnal cycle of shallow cumulus clouds over land: A single-column model intercomparison study. *Quart. J. Roy. Meteor. Soc.*, **130**, 3339–3364, https://doi.org/10.1256/qj.03.122.

Maronga, B., and S. Raasch, 2013: Large-eddy simulations of surface heterogeneity effects on the convective boundary layer during the LITFASS-2003 experiment. *Bound.-Layer Meteor.*, **146**, 17–44, https://doi.org/10.1007/s10546-012-9748-z.

Neggers, R. A. J., 2015: Exploring bin-macrophysics models for moist convective transport and clouds. *J. Adv. Model. Earth Syst.*, **7**, 2079–2104, https://doi.org/10.1002/2015MS000502.

——, A. P. Siebesma, and H. J. J. Jonker, 2002: A multiparcel model for shallow cumulus convection. *J. Atmos. Sci.*, **59**, 1655–1668, https://doi.org/10.1175/1520-0469(2002)059<1655:AMMFSC>2.0.CO;2.

——, J. D. Neelin, and B. Stevens, 2007: Impact mechanisms of shallow cumulus convection on tropical climate dynamics. *J. Climate*, **20**, 2623–2642, https://doi.org/10.1175/JCLI4079.1.

——, M. Köhler, and A. C. M. Beljaars, 2009: A dual mass flux framework for boundary layer convection. Part I: Transport. *J. Atmos. Sci.*, **66**, 1465–1487, https://doi.org/10.1175/2008JAS2635.1.

Ooyama, K., 1971: A theory on parameterization of cumulus convection. *J. Meteor. Soc. Japan*, **49A**, 744–756, https://doi.org/10.2151/jmsj1965.49A.0_744.

Park, S., 2014: A unified convection scheme (UNICON). Part I: Formulation. *J. Atmos. Sci.*, **71**, 3902–3930, https://doi.org/10.1175/JAS-D-13-0233.1.

Plank, V. G., 1969: The size distribution of cumulus clouds in representative Florida populations. *J. Appl. Meteor.*, **8**, 46–67, https://doi.org/10.1175/1520-0450(1969)008<0046:TSDOCC>2.0.CO;2.

Plant, R. S., and G. C. Craig, 2008: A stochastic parameterization for deep convection based on equilibrium statistics. *J. Atmos. Sci.*, **65**, 87–105, https://doi.org/10.1175/2007JAS2263.1.

Rauber, R. M., and Coauthors, 2007: Rain in shallow cumulus over the ocean: The RICO campaign. *Bull. Amer. Meteor. Soc.*, **88**, 1912–1928, https://doi.org/10.1175/BAMS-88-12-1912.

Romps, D. M., and Z. Kuang, 2010: Nature versus nurture in shallow convection. *J. Atmos. Sci.*, **67**, 1655–1666, https://doi.org/10.1175/2009JAS3307.1.

——, and A. B. Charn, 2015: Sticky thermals: Evidence for a dominant balance between buoyancy and drag in cloud updrafts. *J. Atmos. Sci.*, **72**, 2890–2901, https://doi.org/10.1175/JAS-D-15-0042.1.

Sakradzija, M., A. Seifert, and T. Heus, 2015: Fluctuations in a quasi-stationary shallow cumulus cloud ensemble. *Nonlinear Processes Geophys.*, **22**, 65–85, https://doi.org/10.5194/npg-22-65-2015.

——, ——, and A. Dipankar, 2016: A stochastic scale-aware parameterization of shallow cumulus convection across the convective gray zone. *J. Adv. Model. Earth Syst.*, **8**, 786–812, https://doi.org/10.1002/2016MS000634.

Seifert, A., and K. D. Beheng, 2001: A double-moment parameterization for simulating autoconversion, accretion and self-collection. *Atmos. Res.*, **59–60**, 265–281, https://doi.org/10.1016/S0169-8095(01)00126-0.

Shin, H. H., and J. Dudhia, 2016: Evaluation of PBL parameterizations in WRF at subkilometer grid spacings: Turbulence statistics in the dry convective boundary layer. *Mon. Wea. Rev.*, **144**, 1161–1177, https://doi.org/10.1175/MWR-D-15-0208.1.

Shutts, G. J., and T. N. Palmer, 2007: Convective forcing fluctuations in a cloud-resolving model: Relevance to the stochastic parameterization problem. *J. Climate*, **20**, 187–202, https://doi.org/10.1175/JCLI3954.1.

Siebesma, A. P., and J. W. M. Cuijpers, 1995: Evaluation of parametric assumptions for shallow cumulus convection. *J. Atmos. Sci.*, **52**, 650–666, https://doi.org/10.1175/1520-0469(1995)052<0650:EOPAFS>2.0.CO;2.

——, and J. Teixeira, 2000: An advection-diffusion scheme for the convective boundary layer: Description and 1D results. Preprints, *14th Symp. on Boundary Layer and Turbulence*, Aspen, CO, Amer. Meteor. Soc., 133–140.

——, and Coauthors, 2003: A large eddy simulation intercomparison study of shallow cumulus convection. *J. Atmos. Sci.*, **60**, 1201–1219, https://doi.org/10.1175/1520-0469(2003)60<1201:ALESIS>2.0.CO;2.

——, P. M. M. Soares, and J. Teixeira, 2007: A combined eddy-diffusivity mass-flux approach for the convective boundary layer. *J. Atmos. Sci.*, **64**, 1230–1248, https://doi.org/10.1175/JAS3888.1.

Simpson, J., and V. Wiggert, 1969: Models of precipitating cumulus towers. *Mon. Wea. Rev.*, **97**, 471–489, https://doi.org/10.1175/1520-0493(1969)097<0471:MOPCT>2.3.CO;2.

Skamarock, W. C., 2004: Evaluating mesoscale NWP models using kinetic energy spectra. *Mon. Wea. Rev.*, **132**, 3019–3032, https://doi.org/10.1175/MWR2830.1.

Soares, P. M. M., P. M. A. Miranda, A. P. Siebesma, and J. Teixeira, 2004: An eddy-diffusivity/mass-flux parametrization for dry and shallow cumulus convection. *Quart. J. Roy. Meteor. Soc.*, **130**, 3365–3383, https://doi.org/10.1256/qj.03.223.

Stevens, B., and A. Seifert, 2008: Understanding macrophysical outcomes of microphysical choices in simulations of shallow cumulus convection. *J. Meteor. Soc. Japan*, **86A**, 143–162, https://doi.org/10.2151/jmsj.86A.143.

——, C.-H. Moeng, and P. P. Sullivan, 1999: Large-eddy simulations of radiatively driven convection: Sensitivities to the representation of small scales. *J. Atmos. Sci.*, **56**, 3963–3984, https://doi.org/10.1175/1520-0469(1999)056<3963:LESORD>2.0.CO;2.

——, and Coauthors, 2005: Evaluation of large-eddy simulations via observations of nocturnal marine stratocumulus. *Mon. Wea. Rev.*, **133**, 1443–1462, https://doi.org/10.1175/MWR2930.1.

Sušelj, K., J. Teixeira, and G. Matheou, 2012: Eddy diffusivity/mass flux and shallow cumulus boundary layer: An updraft PDF multiple mass flux scheme. *J. Atmos. Sci.*, **69**, 1513–1533, https://doi.org/10.1175/JAS-D-11-090.1.

——, ——, and D. Chung, 2013: A unified model for moist convective boundary layers based on a stochastic eddy-diffusivity/mass-flux parameterization. *J. Atmos. Sci.*, **70**, 1929–1953, https://doi.org/10.1175/JAS-D-12-0106.1.

Teixeira, J., and Coauthors, 2008: Parameterization of the atmospheric boundary layer: A view from just above the inversion. *Bull. Amer. Meteor. Soc.*, **89**, 453–458, https://doi.org/10.1175/BAMS-89-4-453.

Tiedtke, M., 1989: A comprehensive mass flux scheme for cumulus parameterization in large-scale models. *Mon. Wea. Rev.*, **117**, 1779–1800, https://doi.org/10.1175/1520-0493(1989)117<1779:ACMFSF>2.0.CO;2.

Turner, J. S., 1962: The ''starting plume'' in neutral surroundings. *J. Fluid Mech.*, **13**, 356–368, https://doi.org/10.1017/S0022112062000762.

vanZanten, M. C., and Coauthors, 2011: Controls on precipitation and cloudiness in simulations of trade-wind cumulus as observed

during RICO. *J. Adv. Model. Earth Syst.*, **3**, M06001, https://doi.org/10.1029/2011MS000056.

Vial, J., J.-L. Dufresne, and S. Bony, 2013: On the interpretation of inter-model spread in CMIP5 climate sensitivity estimates. *Climate Dyn.*, **41**, 3339–3362, https://doi.org/10.1007/s00382-013-1725-9.

Wagner, T. M., and H.-F. Graf, 2010: An ensemble cumulus convection parameterization with explicit cloud treatment. *J. Atmos. Sci.*, **67**, 3854–3869, https://doi.org/10.1175/2010JAS3485.1.

Wyngaard, J. C., 2004: Toward numerical modeling in the ''terra incognita.'' *J. Atmos. Sci.*, **61**, 1816–1826, https://doi.org/10.1175/1520-0469(2004)061<1816:TNMITT>2.0.CO;2.

Yanai, M., S. Esbensen, and J.-H. Chu, 1973: Determination of bulk properties of tropical cloud clusters from large-scale heat and moisture budgets. *J. Atmos. Sci.*, **30**, 611–627, https://doi.org/10.1175/1520-0469(1973)030<0611:DOBPOT>2.0.CO;2.

Zhou, B., J. S. Simon, and F. K. Chow, 2014: The convective boundary layer in the terra incognita. *J. Atmos. Sci.*, **71**, 2545–2563, https://doi.org/10.1175/JAS-D-13-0356.1.